Real-Time Prediction of Power Electronic Device Temperatures Using PRBS-Generated Frequency-Domain Thermal Cross Coupling Characteristics

Jonathan N. Davidson, David A. Stone, and Martin P. Foster

***Abstract*—This paper presents a technique to predict the temperature response of a multielement thermal system based on the thermal cross coupling between elements. The complex frequency-domain cross coupling of devices is first characterized using a pseudorandom binary sequence technique. The characteristics are then used to predict device temperatures for a known input power waveform using a discrete Fourier transform-based technique. The resulting prediction shows good agreement with an example practical system used for evaluation. To reduce the computational complexity of the initial method, a digital infinite impedance response (IIR) filter is fitted to each cross coupling characteristic. A high correlation fit is demonstrated that produces a near-identical temperature response compared to the initial procedure while requiring fewer mathematical operations. Experimental validation on the practical system shows good agreement between IIR filter predictions and practical results. It is further demonstrated that this agreement can be substantially improved by taking feedback from an internal reference temperature. Additionally, the proposed IIR filter technique allows the efficient calculation of future device temperatures based on simulated input, facilitating future temperature predictions.**

***Index Terms*—Infinite impedance response (IIR) digital filters, prediction methods, pseudonoise processes, spectroscopy, thermal variables measurement.**

I. Introduction

THE design of power electronics is increasingly constrained by space, weight, and temperature considerations. In many applications, significant emphasis is placed on these constraints due to the environment in which the system is to operate. This is particularly true of power converters for electric vehicles (EVs), where the constraints are more severe than in static applications [1]. In EV applications, for example, electrical power converters must be lightweight, fit into the small space available, and operate in an enclosed environment with high ambient temperature and limited natural air flow. Ideally, the design of systems would include the use of well-spaced components to reduce thermal cross coupling and use large heatsinks to reduce the thermal resistance to ambient. However, this leads to increased weight, size, and cost, which is contrary to the design constraints. As a result, the engineer is forced to place power components in close proximity with minimal heatsinking.

Despite the increasing use of efficient converter topologies and components, advanced thermal design and monitoring of the converter is of substantial importance to prevent overheating. Of particular interest to the engineer is the thermal cross coupling between devices. When considered in isolation, the temperature of a device is a function of only its own power dissipation waveform and the cooling system employed. In a compact system, however, its temperature is also heavily dependent on dissipation waveforms in other components. We term this dependency the cross coupling between the components.

The importance of cross coupling is demonstrated by Fig. 1, which shows two thermal images of four power devices (1, 2, 3, 4) mounted on a heatsink. If device 2 dissipates 95 W, then its temperature rises to 113 °C, which is acceptable for a silicon device. However, if both devices 2 and 4 each dissipate 95 W simultaneously, the temperature at each device rises beyond 134 °C, which is potentially damaging to many silicon devices. The 21 °C difference in temperature results from cross coupling that would not be predicted by simple thermal modeling. This demonstrates the need to take cross coupling effects into account for accurate thermal modeling.

Extensive literature exists on the identification of cross coupling characteristics. Many research papers characterize the thermal cross coupling by fitting an electrical equivalent circuit of resistors and capacitors to the system [2]–[4]. Other methods are also used. Evans, for example, describes the development of a model based on state-space differential equations of the heat equation, which is simplified using a computer algorithm [5].

Once identified, cross coupling characteristics can be used to predict the temperature at each system element due to the power dissipations in all elements. These prediction methods are important in power electronics because they allow a design to be evaluated in terms of its compliance with the rated maximum temperature of elements under a range of operating conditions. Brückner and Bernet [2] report one such temperature estimation technique for a voltage-source converter module. By constructing an electrical analogue for the thermal system and calculating power input from electrical characteristics, the junction

Manuscript received October 30, 2013; revised April 2, 2014; accepted March 10, 2014. Date of publication June 24, 2014; date of current version January 16, 2015. Recommended for publication by Associate Editor B. Ferreira.

The authors are with the Department of Electronic and Electrical Engineering, The University of Sheffield, Sir Frederick Mappin Building, Mappin Street, Sheffield S1 3JD, U.K. (e-mail: jonathan.davidson@sheffield.ac.uk; d.a.stone@sheffield.ac.uk; m.p.foster@sheffield.ac.uk).

Color versions of one or more of the figures in this paper are available online at http://ieeexplore.ieee.org.

Digital Object Identifier 10.1109/TPEL.2014.2331285

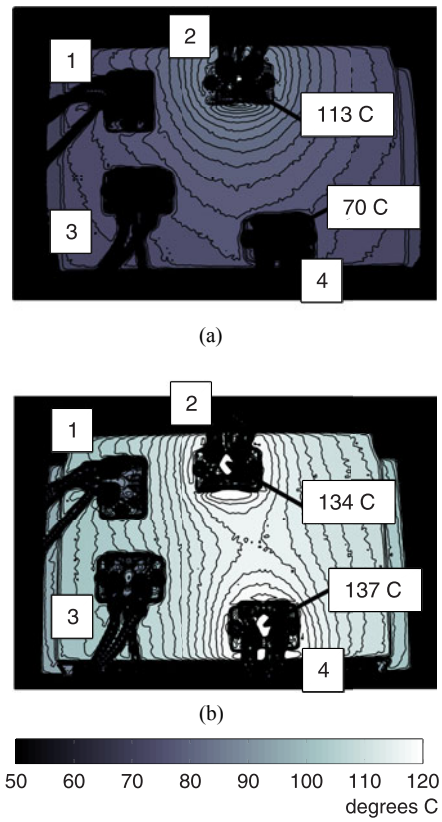

Fig. 1. Thermal images of four devices mounted on a heatsink with temperature of device 2 indicated. (a) Device 2 dissipating alone (b) Both device 2 and device 4 dissipating.

temperatures of the semiconductor devices are estimated. In this case, however, temperature is not calculated with respect to time but rather the temperature at each element for each operating condition is evaluated. In a system with variable operating conditions, a method that predicts the temperature at a given time for an arbitrary dissipation profile is required.

Systems that predict the temperature response in real time are of particular significance. In these cases, techniques such as active cooling may be used to maintain system parameters within tolerances. This concept has been applied extensively for on-chip temperature management in the very large scale integration sector. Wang *et al.* [6], for example, uses model-predictive control to calculate the temperature and attempt to hold it at a set point by varying power consumption. This approach has applications in power electronics, where the maximum element temperatures are constraints to the safe operating envelope. Wang *et al.* [4] report a method that uses a grid of resistors, capacitors, and current sources to model a planar microchip. By constructing a finite-difference equation, the temperature response at several points can be estimated in real time for arbitrary power input. This estimate is improved using error compensation from a limited number of on-board temperature sensors. Similarly, Musallam and Johnson [7] use a combination of the practical and simulated temperature response to a step power input to generate parameters for a Laplace-domain model. By transforming the model into the time domain and converting to a difference

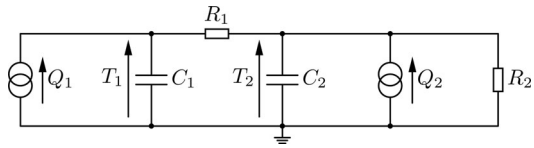

Fig. 2. Schematic of multiple heat sources and temperature measurements.

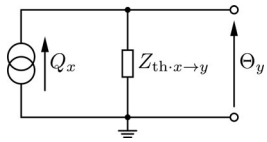

Fig. 3. Norton equivalent circuit of the thermal circuit between heat source x and measurement point y.

equation, the temperature due to an arbitrary power input may be computed in real time. In [7], the model is parameterized and the difference equations computed for each pair of system elements; hence, the effect of cross coupling is explicitly taken into account.

In recent years, similar approaches have been applied to power electronics. For example, James *et al.* [3] have reported using a step function to evaluate the auto- and cross coupling between elements of multichip power electronic module and fits these characteristics to a Foster network. The resulting model is used to predict the temperature response for an arbitrary power input.

In this paper, the cross coupling is directly measured for use in temperature prediction using a pseudorandom binary sequence (PRBS) technique. To provide real-world focus, the thermal design of a typical H-bridge converter is used for evaluation, an application where there are significant thermal constraints [8]. This paper expands existing work presented at European Conference on Power Electronics and Applications Lille 2013 [9] by providing a more detailed analysis of the technique and demonstrating greater computational efficiency by fitting infinite impulse response (IIR) filters to the cross coupling characteristics.

II. Cross Coupling

A. Definition

A thermal system can be modeled as an electrical equivalent circuit, consisting of resistors and capacitors. Fig. 2 shows a typical thermal equivalent circuit between multiple heat sources (represented as current sources) and temperature readings (represented as voltages).

The topology of the network model differs both between systems and with the type of modeling used; however, like all linear two-port systems, the relationship between a single power source and single temperature reading can be simplified into a Norton equivalent circuit with impedance dependent on frequency. Fig. 3 shows the Norton circuit between heat source x and temperature measurement point y. In this study, we use Q, Z_{th}, and Θ to refer to the frequency-domain representations of heat flux, thermal impedance, and temperature, respectively. In

addition, all temperatures reported are relative to ambient that we represent symbolically as an earth connection.

The cross coupling $Z_{\mathrm{th}\cdot x\to y}$ is the complex frequency-domain transfer impedance between heat source x and measurement y. By applying Ohm's law and the theory of superposition, the temperature at all measurement points due to all device dissipations can be expressed in matrix form as shown in (1). The $n \times m$ thermal impedance matrix is the combined characteristics of the entire system

$$\begin{pmatrix} \Theta_1 \\ \vdots \\ \Theta_m \end{pmatrix} = \begin{pmatrix} Z_{\mathrm{th}\cdot 1\to 1} & \cdots & Z_{\mathrm{th}\cdot n\to 1} \\ \vdots & \ddots & \vdots \\ Z_{\mathrm{th}\cdot 1\to m} & \cdots & Z_{\mathrm{th}\cdot n\to m} \end{pmatrix} \begin{pmatrix} \mathrm{Q}_1 \\ \vdots \\ \mathrm{Q}_n \end{pmatrix} \quad (1)$$

where n and m are the number of devices and temperature measurement points in the system, respectively. In this study, both temperature measurement and power input are taken for each of the power devices, therefore $n = m$. Equation (1) must be evaluated for each frequency to generate the complete temperature response.

B. Generation of Cross Coupling Characteristics by PRBs

To characterize $Z_{\mathrm{th}\cdot x\to y}$ between components *x* and *y* over a frequency range, system identification techniques are used. The easiest to implement is impedance spectroscopy wherein a pure sine wave power excitation signal is applied to the system and the amplitude and phase of the temperature response are recorded. For thermal systems, which have very long time constants, this technique is very time consuming since at least two cycles per reading are required to overcome transient effects. A typical thermal spectrum of five readings per decade between 10 μHz and 0.1 Hz would, therefore, take at least six days.

Consequently, in this study we use an alternative method of system identification: a PRBS technique. For brevity, only a brief overview of the use of PRBS is provided in this study. For more detail, the theory behind these sequences and the techniques derived from them are described by Davies [10].

An alternative to the PRBS is to apply a step function of power dissipation to the thermal system and measure the transient response, which can then be fitted to a Foster Network [5]. This technique has two main limitations. First, the Foster networks characterized can only model self-impedance because they are one-port networks. In this study, however, transfer impedance is required that would demand the use of a more general network such as a two-port Cauer network [11]. Second, the conversion from a thermal transient to a frequency-domain representation (required for the technique proposed in this study) is difficult because the conversion process is very sensitive to noise, particularly at higher frequencies, as shown by Salleras *et al.* [12]. PRBS is, therefore, preferred over transient response measurement for cross coupling characterization.

PRBS techniques apply a specially generated excitation signal, which has an almost flat power spectrum over the band of frequencies given in (2). By applying this signal as an input-power waveform to a thermal system and measuring the resulting temperature waveform, the system can be characterized over the frequency band. In this way, the response of the system can be determined over a range of frequencies simultaneously

$$\frac{\omega_p}{N} \le \omega \le \frac{\omega_p}{2.3} \quad (2)$$

where ω is the valid frequency band, ω_P is the clock frequency of the PRBS, and N is the number of periods of ω_p that are present in a single sequence. There are many techniques to generate PRBSs, each with various parameters to control sequence length, bandwidth, and phase characteristics [10]. In this study, we use an 8-bit PRBS generated by a linear shift feedback register with a four-input exclusive-NOR gate tapped from bits 5 to 8 providing the feedback, as shown in Fig. 4. For an n-bit shift register, the sequence length N, is $2^n - 1$. In this study, where an 8-bit PRBS is used, $N = 255$.

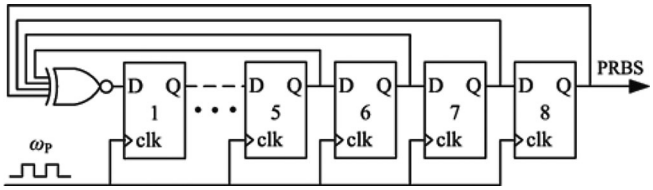

Fig. 4. Implementation of an 8-bit PRBS using a linear-shift feedback register.

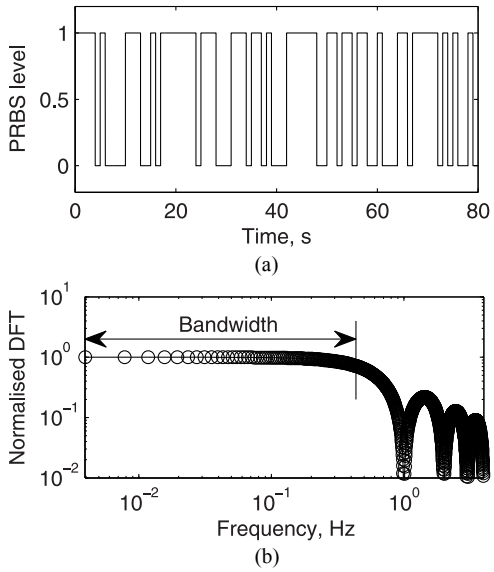

Fig. 5. (a) Time and (b) frequency-domain representations of the 8-bit PRBS clocked at 1 Hz.

The PRBS is a two-level signal with pseudorandomly spaced transitions. A section of the 8-bit PRBS and the frequency-domain representation generated using the discrete Fourier transform (DFT) are shown in Fig. 5(a) and (b), respectively. The cross coupling spectrum between two points in a system under test is generated by applying a PRBS input-power waveform to device x and measuring the temperature response at point y and then taking the quotients of the DFTs of power and temperature as shown in

$$Z_{\mathrm{th}\cdot x\to y}(\omega) = \frac{\mathcal{F}(\theta_y(t))}{\mathcal{F}(q_x(t))} = \frac{\Theta_y(\omega)}{Q_x(\omega)} \quad (3)$$

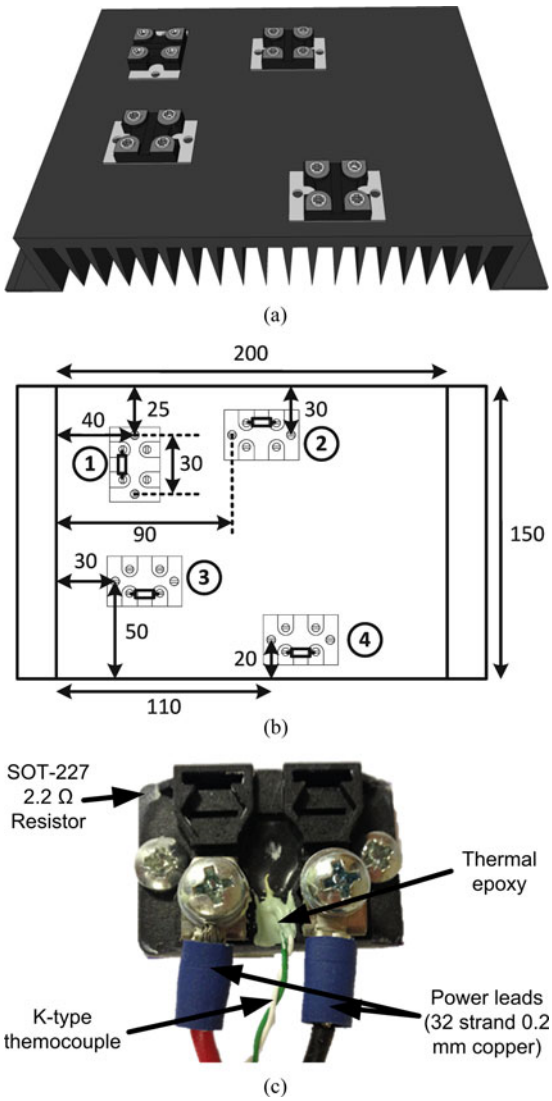

Fig. 6. Heatsink arrangement. (a) Three-dimensional view. (b) Plan view with measurements in millimetres and resistor number circled. (c) Close up of individual device.

where $\mathcal{F}$ is the DFT operator and ω is angular frequency. θ_y and q_x are the time-domain temperatures and power readings at points *y* and *x*, respectively. PRBS techniques are used in numerous applications including battery modeling [13], parameter estimation in electric generators [14], and characterization of thermal systems [15], [16]. By applying them to thermal cross coupling in this study, experimental time is reduced, therefore, making real-time temperature prediction based on frequency-domain characteristics practical.

III. Experimental Arrangement

A typical arrangement for power electronics is used to demonstrate the techniques outlined in this paper. An H-bridge based multikilowatt converter, with four SOT-227 packaged power devices mounted on a passively cooled 0.47-K/W heatsink, is selected. The power devices are placed irregularly as shown in Fig. 6 to reflect the fact that the placement of devices is a compromise between thermal and electrical design [17]. The MOSFETs in the design are substituted for power resistors since this allows the power dissipated to be controlled more easily and removes the need to construct a complex control circuit. A power controller determines the instantaneous dissipation in the devices, which can be set to match the operational losses in a converter so that the thermal characteristics of the system are unchanged.

A thermocouple is attached with thermal epoxy resin to the top of each package in the recess directly above each resistor to measure the device temperature as shown in Fig. 6(c). In this study, Θ_1 to Θ_4 and Q_1 to Q_4 refer to the frequency-domain temperature and power dissipation in devices 1 to 4, as identified in Fig. 6(b), respectively.

Temperature measurement was performed using a LabJack U6 measuring to an effective resolution of 0.006 K at 25 samples per second, giving the system a maximum accessible bandwidth of 12.5 Hz. The rise time of the thermocouples is 0.1 s, while the bandwidth of the waveform generator and power dissipation controller are in excess of 1 kHz. Overall, the system bandwidth is, therefore, at least 10 Hz. In this study, the maximum frequency used is 0.1 Hz, a value sufficiently below the system bandwidth as to make results independent of the measurement system. The power spectral density of the noise from the thermocouple measurement was 1.4×10^{-4} K^2/Hz.

IV. Measurement of Thermal Cross Coupling

To measure the thermal cross coupling between the devices, a PRBS was applied to each resistor using the technique described in [13]. Each device in turn was excited with a 0.004 Hz 8-bit PRBS with an amplitude 95 W and the resulting temperature responses at all devices were logged. Each experiment was repeated with three cycles of a 0.1-Hz PRBS to extend the valid frequency range. From (2), the valid frequency band of the PRBS is, therefore, 15.6 μHz to 43 mHz.

Fig. 7 shows the cross coupling calculated between each pair of devices on the heatsink. In addition, the thermal autocoupling $Z_{\mathrm{th}\cdot x\to x}$ is measured and indicated. This is the temperature rise in a device due to its own dissipation and is greater in value than the cross coupling between devices, with the difference being particularly large at high frequency.

The cross coupling characteristics between different devices are broadly similar in shape because they are mounted on the same heatsink under similar conditions. However, there are notable differences in the coupling between different devices. The coupling between devices 1 and 3, for example, is significantly elevated compared to other devices [evident in Fig. 7(a) and (b)]. This is due to the close proximity of the devices. Similarly, the coupling between devices 1 and 2 is counterintuitively lower than that of devices 1 and 3 even though they are physically separated by the same distance. This is due to the heatsink's fin arrangement lowering the thermal resistance between devices 1 and 3, but not devices 1 and 2.

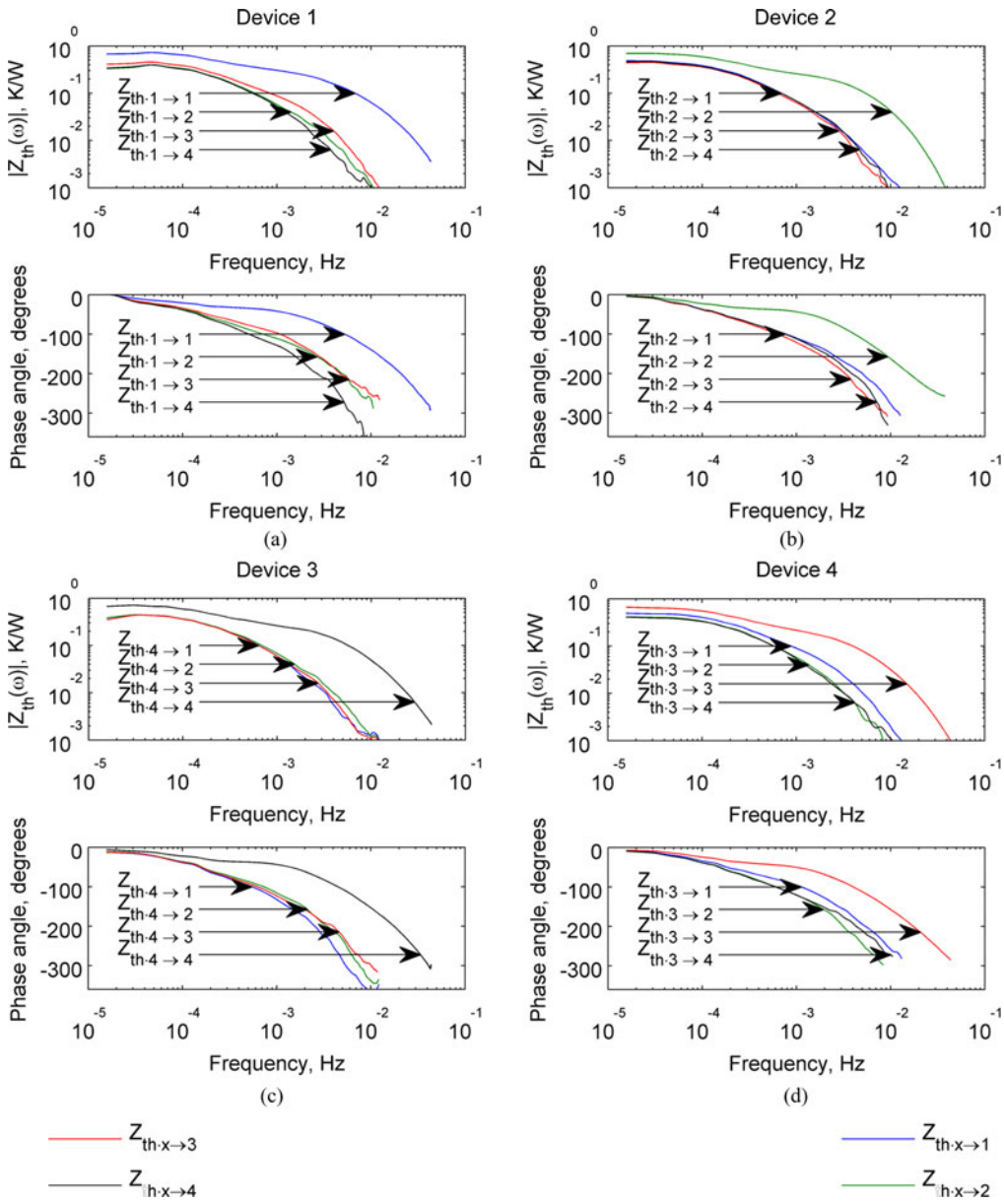

Fig. 7. Cross coupling between components. (a) From device 1. (b) From device 2. (c) From device 3. (d) From device 4.

V. Prediction of Temperatures

A. Prediction Using Frequency-Domain Data

Having obtained the cross coupling characteristics between each pair of devices, the temperature response of each device due to arbitrary input-power waveforms in any combination of the devices can be predicted. In this section, we examine how this prediction can be made using frequency-domain analysis of the input powers and cross coupling. Fig. 8 shows the procedure for generating such predictions using the DFT. First, for each pair of devices *x* and *y*, the DFT of the temperature at device *y* due to the power dissipation in device *x* is calculated and termed $\Theta_{y(x)}$. Subsequently, the temperature at each device is calculated by summing the contributions from each power source and evaluating the inverse DFT. This procedure is described in detail later.

The input power $q_x\ (t)$, which is to be analyzed using this procedure will be defined over the finite time period $0 \leq t \leq t_{\max}$. However, it is not possible to calculate the temperature response over the same period using this power waveform directly because the DFT, which is used in this procedure, assumes that its input is periodic. Assuming the temperature difference from each device to ambient is initially zero, the output of the inverse DFT used in processing must also begin and end with value zero. To achieve this, the simulation period is extended and the input-power waveform $q_x\ (t)$ is padded with zeros such that any

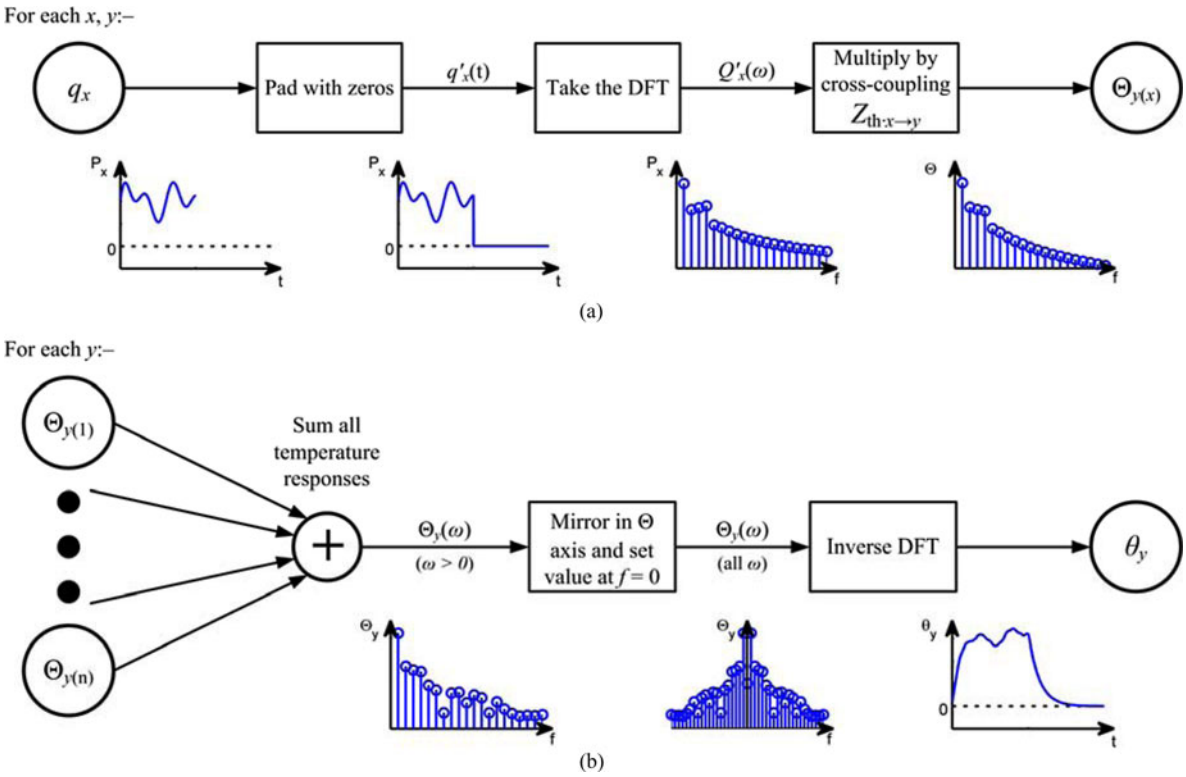

Fig. 8. Procedure for calculating the temperature response from cross coupling data with example waveforms shown. (a) For calculating the frequency-domain response at y due to individual heat source x. (b) For calculating the time-domain response at y due to all heat sources.

stored thermal energy at time $t_{\max}$ (due to the input power) is dissipated to ambient before the end of the simulation period, as shown in (4), thereby fulfilling the DFT's periodicity criterion

$$q'_x(t) = \begin{cases} q_x(t), & t \le t_{\max} \\ 0, & t_{\max} < t \le t_{\max} + 3\tau_{\max} \end{cases} \tag{4}$$

where $t_{\max}$ is the maximum time for which $q_x(t)$ is defined, and $\tau_{\max}$ is an estimate of the slowest time constant of the system. To calculate the temperature at device y, the DFT ($\mathcal{F}$) of the padded input power is taken and multiplied by the cross coupling between device y and each of the other devices at every frequency in the DFT to find $\Theta_{y(x)}$ for each pair. The temperature response is the sum of these temperature DFTs as shown in (5). This is a single line of the thermal impedance matrix equation given in (1). Because the valid frequency range of the cross coupling $Z_{th\cdot x\to y}$ may be smaller than the frequency range of the input power, $Z_{th\cdot x\to y}$ is extended. $Z_{th\cdot x\to y}(\omega_{\min})$ is, therefore, used for frequencies in the input power lower than the minimum $\omega_{\min}$, for which $Z_{th\cdot x\to y}$ is defined. Similarly, the cross coupling is assumed to be zero for frequencies higher than the maximum defined frequency $\omega_{\max}$. This is expressed mathematically in (6) below

$$\Theta_y[k] = \sum_x \mathcal{F}(q'_x(t))[k] \cdot Z_{th\cdot x\to y}(\omega) \tag{5}$$

$$Z_{th\cdot x\to y}(\omega) = \begin{cases} Z_{th\cdot x\to y}(\omega_{\min}), & 0 < \omega < \omega_{\min} \\ Z_{th\cdot x\to y}(\omega), & \omega_{\min} \le \omega \le \omega_{\max} \\ 0, & \omega > \omega_{\max} \end{cases} \tag{6}$$

where $k = \omega(n_s - 1)/\omega_s$ is the discrete frequency index, ω_s is the sampling rate, and n_s is the number of samples. The aforesaid description is for the positive frequencies present in the DFT. The negative frequency response can be obtained using (7). Because the temperature waveform we are producing is real, its DFT at negative frequencies is the complex conjugate mirror of its DFT at positive frequencies [18]. The values at negative frequencies in the DFT are, therefore, calculated according to

$$\Theta_y[-k] = \Theta_y^*[k]. \tag{7}$$

The value at frequency zero ($\Theta_y[0]$) is proportional to the average value of θ_y and, therefore, the average temperature. This can be seen from the synthesis and analysis equations of the DFT [18]. In this study, we calculate the temperature difference from ambient. Because the system is initially at ambient, $\Theta_y[0]$ is set such that the initial temperature difference is zero, according to

$$\Theta_y[0] = -\sum_{\substack{k=-(n_s-1)/2 \\ k\neq 0}}^{(n_s-1)/2} \Theta_y[k]. \tag{8}$$

The inverse DFT ($\mathcal{F}^{-1}$) is then taken and the time-domain temperature signal obtained, producing the final expression for the temperature response θ_y, as shown in

$$\theta_y(t) = \mathcal{F}^{-1}(\Theta_y[k]). \tag{9}$$

To validate the technique, devices 2 and 4 were set to simultaneously dissipate 95-W square waves at 2 and 0.2 mHz, respectively. The temperature responses of all devices were

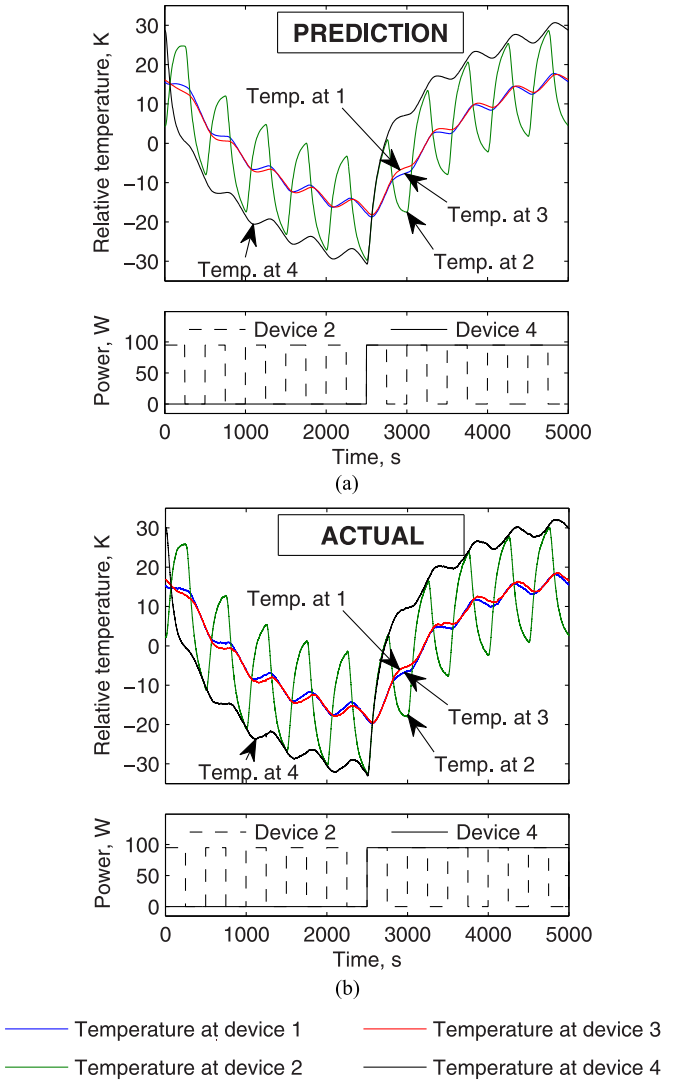

Fig. 9. (a) Predicted and (b) measured experimental responses to 0.2–2-mHz square wave dissipation.

predicted using the procedure described earlier and are shown in Fig. 9(a). In this case, we have assumed that the power input is periodic and that all transients have passed and have therefore not added padding according to (4). The waveforms were also applied experimentally to the example heatsink and the temperature response recorded over one cycle once steady state was reached as shown in Fig. 9(b). For simplicity, the dc component of temperature was neglected in this experiment.

The two plots show good agreement with each other. The correlation coefficient r^2 is greater than 0.99 and the root-mean-square error is less than 2.4 K or 3% of the total range for each waveform, indicating that the cross coupling method proposed is effective for temperature prediction.

B. Improved Computational Efficiency by Fitting a Digital IIR Filter

The direct use of frequency-domain characteristics discussed earlier is computationally intensive since the calculation of forward and inverse DFTs are required. In order to provide a real-time prediction of temperature, the whole input power waveform must be analyzed and the entire temperature response generated. For a long power profile, the computational power required approaches that of a desktop PC. Ideally, the proposed technique could be implemented on an embedded system installed alongside a power converter to monitor input power and predict the temperature accordingly. A microcontroller-based system would be particularly suitable as modern power electronics converters and drives typically already contain such a device [19].

The usual approach to simplifying a thermal system is to model it as an equivalent circuit of resistors, capacitors, and current sources, known as a lumped parameter model [20]. These models can be constructed directly by calculation based on the geometry of devices and their heatsinks without reference to experimental data. Lumped parameter models are commonly used for real-time temperature predictions in a number of applications including simulation of buildings and their heating systems [21] and electrical machines [22]. Their simplicity means they are easy to implement on embedded systems. Lumped parameter models have also been applied to temperature predictions in power electronic systems. For example, Holmes *et al.* [23] presents a method using a simple equivalent circuit and a closed-loop Luenberger observer system to predict device temperatures in real time. The effectiveness of this model is limited, however, as the equivalent circuit must be formulated and its component values populated before it can be used to make predictions. Although the observer system proposed in [23] can correct scaling errors, wrongly arranged components, or situations, where components have erroneous relative values, limit the effectiveness of the design.

Alternatively, the thermal impedance of a system can be modeled using a simplified electrical equivalent circuit. For example, James *et al.* [3] model the cross coupling in a thermal system by fitting a Foster network to the step response between each pair of devices. While this approach has the advantage of rapidly generating a simplified equivalent circuit, it is subject to the limitations on step response characterization discussed in Section IIA. To embed a temperature predictor based on such a model into a microcontroller, the equivalent circuit must undergo transient analysis. For a given model, a set of finite-difference equations is produced by applying the trapezium rule to differential equations for each capacitor [24]. These equations are then used iteratively to generate a temperature prediction for an arbitrary input. This method has the disadvantage that the difference equations are not generated directly from the characterization. They must instead be generated from an equivalent circuit model using transient circuit analysis. In the proposed method, the difference equations are directly generated from cross coupling techniques, removing inaccuracy from step-response characterization and avoiding the need for transient circuit analysis.

We propose fitting a digital filter to the cross coupling characteristics. A digital filter is a series of additions and multiplications performed on the current and previous samples of the input-power waveform. Filters are described by two vectors, $\boldsymbol{a}$ and $\boldsymbol{b}$. From [18], the output of the filter may be calculated as

shown in (10). From this equation, simple difference equations can be generated directly [18]

$$\theta[i] = \sum_{\lambda=1}^{G} a_\lambda \theta[i-\lambda] + \sum_{\lambda=0}^{H} b_\lambda q[i-\lambda] \tag{10}$$

where i is the sample number and G and H are the lengths of vectors $\boldsymbol{a}$ and $\boldsymbol{b}$, respectively. The filter is said to be causal because no information from future values is required to calculate the present output value. This is necessary for real-time prediction. The frequency response of the system is

$$Z_{\mathrm{th}}(z) = \frac{\sum_{\lambda=0}^{G} b_\lambda z^{-\lambda}}{1 - \sum_{\lambda=1}^{H} a_\lambda z^{-\lambda}}; \quad z = e^{-\mathrm{j}2\pi\left(\frac{\omega}{\omega_s}\right)} \tag{11}$$

where z is the z-transform variable, j is the imaginary unit, ω_s is the sampling frequency, and ω is the angular frequency.

There are two types of filter available. The finite impulse response (FIR) filter, where $a_\lambda = 0$ for $\lambda \geq 1$, is the simpler but the response to a power input is of finite length since after H zero-input samples the output falls to zero. This type of filter is very easy to implement as only a memory of the previous H samples is required. Its usefulness is limited, however, by the length of the filter commonly necessary to model a real system at a sensible sampling rate and by the group delay that results from a long filter. FIR design techniques also tend to have linear phase [18], which is not generally true of cross coupling.

Alternatively, an IIR filter may be fitted. This filter has arbitrary length $\boldsymbol{a}$ and $\boldsymbol{b}$ vectors that may take any real value. Because the output is fed back, an IIR filter's response to an input waveform is typically infinite in length. In addition, IIR filters are more computationally efficient since they typically require shorter vectors $\boldsymbol{a}$ and $\boldsymbol{b}$ than FIR filters, meaning fewer previous samples have to be stored [18].

In this study, we therefore utilize IIR filters for the cross coupling frequency responses identified. Fitting is based on the MATLAB invfreqz function [26]. This uses the Gauss–Newton iterative method to find vectors $\boldsymbol{a}$ and $\boldsymbol{b}$ that minimize the mean square error between the desired frequency response and the curve fit in (12) to form a stable IIR filter

$$\sum_{k=0}^{n_s-1} \left| Z_{\mathrm{th}}(\omega(k)) - \frac{B(\varphi(k))}{A(\varphi(k))} \right|^2 \tag{12}$$

$$B(\varphi) = \sum_{\lambda=0}^{G} b_\lambda e^{-\mathrm{j}\pi\lambda\varphi}; \quad A(\varphi) = 1 - \sum_{\lambda=1}^{H} a_\lambda e^{-\mathrm{j}\pi\lambda\varphi} \tag{13}$$

$$\varphi(k) = \frac{\pi}{\omega_{\max}} \omega(k) \tag{14}$$

$$\omega(k) = \omega_{\min} \left(\frac{\omega_{\max}}{\omega_{\min}} \right)^{\frac{k}{n_s-1}} \tag{15}$$

where A and B are functions of $\boldsymbol{a}$ and $\boldsymbol{b}$, respectively, given in (13), k is the frequency index, and n_s is the number of samples over which Z_{th} is calculated. For correct weighting of the different frequencies in the minimization of function (12), a logarithmic spread of frequencies is used between $\omega_{\min}$ and $\omega_{\max}$, which are the minimum and maximum frequencies over which Z_{th} is defined, as shown in (15). $\omega(k)$ is the real angular frequency for which $Z_{\mathrm{th}}(\omega)$ is defined. Since the Fourier transform is periodic around the unit circle, $\varphi(\omega)$ is the scaled angular frequency in the range $0 \leq \varphi \leq \pi$. For both ω and φ, negative frequencies are omitted due to symmetry.

This method of minimization was selected since it considers the complex values of the cross coupling, as opposed to the magnitude alone. By doing this, both phase and magnitude are matched closely. Vectors of length 4 and 7 were chosen for $\boldsymbol{a}$ and $\boldsymbol{b}$, respectively, as these values were the smallest that yielded good results. Although the characterization is a computationally intensive procedure, it is performed offline only once.

Fig. 10(a) and (b) shows the typical Bode plots of measured and fitted IIR filter spectra for typical autocoupling ($Z_{\mathrm{th}\cdot x\to x}$) and cross coupling ($Z_{\mathrm{th}\cdot x\to y}$) characteristics, respectively. The agreement between the IIR filter and the measured spectrum is very good in the case of the autocoupling spectrum due to its higher impedance and, therefore, greater noise immunity. The cross coupling spectrum shows reduced agreement at high frequency, particularly in phase, caused by the effect of noise in the original measurement.

Noise in the system results in a noise floor $|Z_{\mathrm{noise}}|$ in the measurement of thermal impedance under which neither the magnitude nor phase can be measured accurately. For the experimental setup in this study, the spectral density of the noise was 4.3×10^{-4} K^2/Hz. Since three repeated sequences of the high-frequency PRBS are averaged, the effective noise is reduced by a factor of 3 to 1.4×10^{-4} K^2/Hz. It has been shown [10] that the spectral density for a unipolar PRBS power waveform with respect to frequency f is

$$\Phi_{\mathrm{PRBS}}(f) = \frac{Q^2}{4f_p} \cdot \frac{N+1}{N} \left[\frac{\sin f\pi/f_p}{f\pi/f_p} \right] \tag{16}$$

where Q is the PRBS amplitude and f_p is the PRBS clock frequency. At the highest frequency in the useable bandwidth, $f = 43$ mHz, the PRBS frequency is $f_p = 0.1$ Hz, and the spectral density is, therefore, $\Phi_{\mathrm{PRBS}}\left(43 \times 10^{-3}\ \mathrm{Hz}\right) = 1.6 \times 10^5$ W^2/Hz. Because the Fourier transform is proportional to the square root of the power spectrum, the impedance measured due to noise alone is, from (3)

$$|Z_{\mathrm{noise}}| = \frac{\sqrt{\Phi_{\mathrm{noise}}}}{\sqrt{\Phi_{\mathrm{PRBS}}}} = 9.4 \times 10^{-5}\ \mathrm{K/W}. \tag{17}$$

For measured impedances approaching this value, noise adversely affects results. For measurement of phase, the effect is more pronounced since the phase angle of noise is random, whereas the amplitude of noise is limited to around $|Z_{\mathrm{noise}}|$. This is the reason for the error seen at low values of thermal impedance in Fig. 10(b). However, since the impedance is low at noise-affected frequencies, the effect of the error on the resulting predictions is negligible. A full explanation of system identification using PRBS in noisy conditions is given in [25].

The temperature response may be calculated using (10) or, alternatively, with the more efficient direct form II implementation

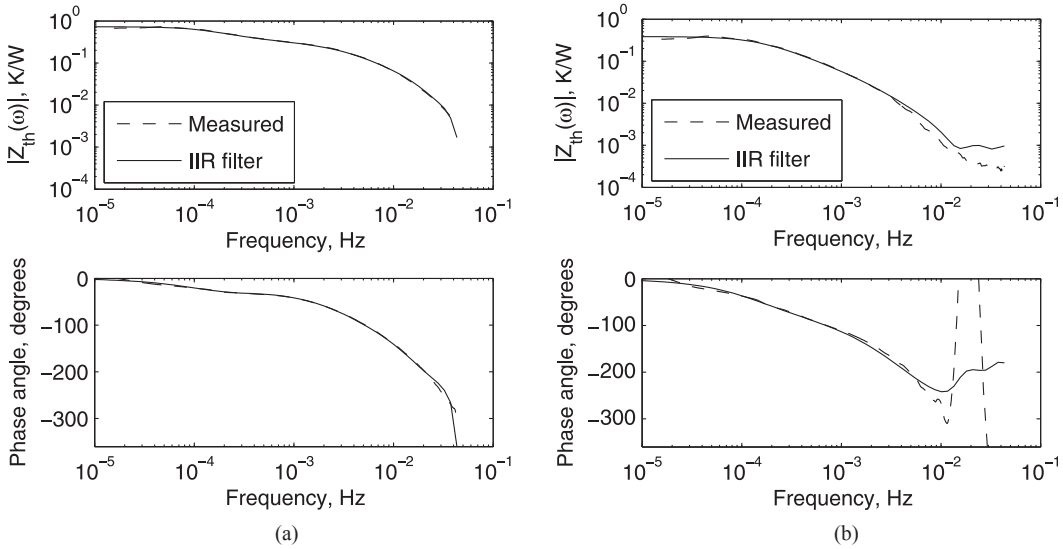

Fig. 10. Typical Bode plots for measured and fitted IIR filter spectra for: (a) autocoupling $Z_{\mathrm{th}\cdot 1\to 1}$ and (b) cross coupling $Z_{\mathrm{th}\cdot 1\to 2}$.

given in [18]. The sampling frequency of the filter is set by the Nyquist limit of the cross coupling according to

$$\omega_s = 2\omega_{\max}. \tag{18}$$

The agreement between temperature predictions made using the direct cross coupling procedure and predictions made from a fitted IIR filter is excellent. Fig. 11(a) and (b) shows predictions for an arbitrary input power waveform [see Fig. 11(e)] using these techniques. For clarity, each of these figures consists of a view of the entire profile on the left and the magnified peak region (where differences are greatest) on the right. The input power waveform is the EU driving cycle [27], where the power demand is variable and becomes larger over time, before dropping to zero. The temperature response is, therefore, a steady but perturbed increase followed by an exponential decay. The root-mean-square difference between the direct cross coupling predictions and the IIR filter predictions is 0.13 K, which is negligible and demonstrates their equivalency. These results are discussed in more detail in Section VI.

C. Real Temperature Feedback

The accuracy of the temperature response can be improved with feedback from a single temperature sensor. By measuring the temperature at one point for which the cross coupling characteristics are known, the difference between the predicted and practical temperature can be calculated. Assuming that this difference is consistent between all the points for which cross coupling is known, the temperature at these points can be accurately predicted according to

$$\Theta'_y = \Theta_{\mathrm{prediction},y} + (\Theta_{\mathrm{real},r} - \Theta_{\mathrm{prediction},r}) \tag{19}$$

where $\Theta_{\mathrm{prediction},r}$ and $\Theta_{\mathrm{real},r}$ are predicted and feedback temperatures at point r, respectively. Θ'_y is the feedback-corrected temperature at point y. This technique can be applied to the IIR filter method described earlier, and for the example heatsink arrangement reported in this paper. For this experiment, we correct the reading using the temperature data for device 3, which is selected due to its central location. The effectiveness of this technique is discussed in Section VI and shown in Fig. 11(c).

D. Temperature Response Extrapolation

Predicting the temperature response to future power input is a useful feature of a temperature control system [23]. For example, if it appears likely that the thermal limits are to be exceeded in the future, actions can be taken to avoid this, such as limiting power, increasing cooling or warning the user. A significant advantage of the IIR filter prediction technique compared to the use of the DFT on cross coupling characteristics directly is the ease with which prediction can be made for simulated input. By duplicating the filter's internal state and inputting simulated input power (perhaps by duplicating recent power dissipation), the temperature at any point in the future can be predicted efficiently and accurately. Since sample rates of less than 10 Hz are typically required for the IIR filter, predicting 1 min ahead will require less than 600 filter iterations. Calculations of the necessary complexity could be performed by a typical microcontoller in a few milliseconds.

VI. Comparison of Techniques

To demonstrate the techniques an arbitrary power waveform is used. A power cycle, based on a vehicle running the European driving cycle waveform [27], is selected as it is well known and is of an appropriate length for the time constants of the heatsink arrangement used in this study and is sufficiently arbitrary to permit the easy evaluation of the techniques. For simplicity, the power handling requirement is assumed to be proportional to the vehicle velocity described in the driving cycle.

Fig. 11(a)–(c) shows the predicted temperature response of the example heatsink arrangement to the input power waveform in Fig. 11(e). To validate the results, this input power waveform was applied practically to the example system and the resulting

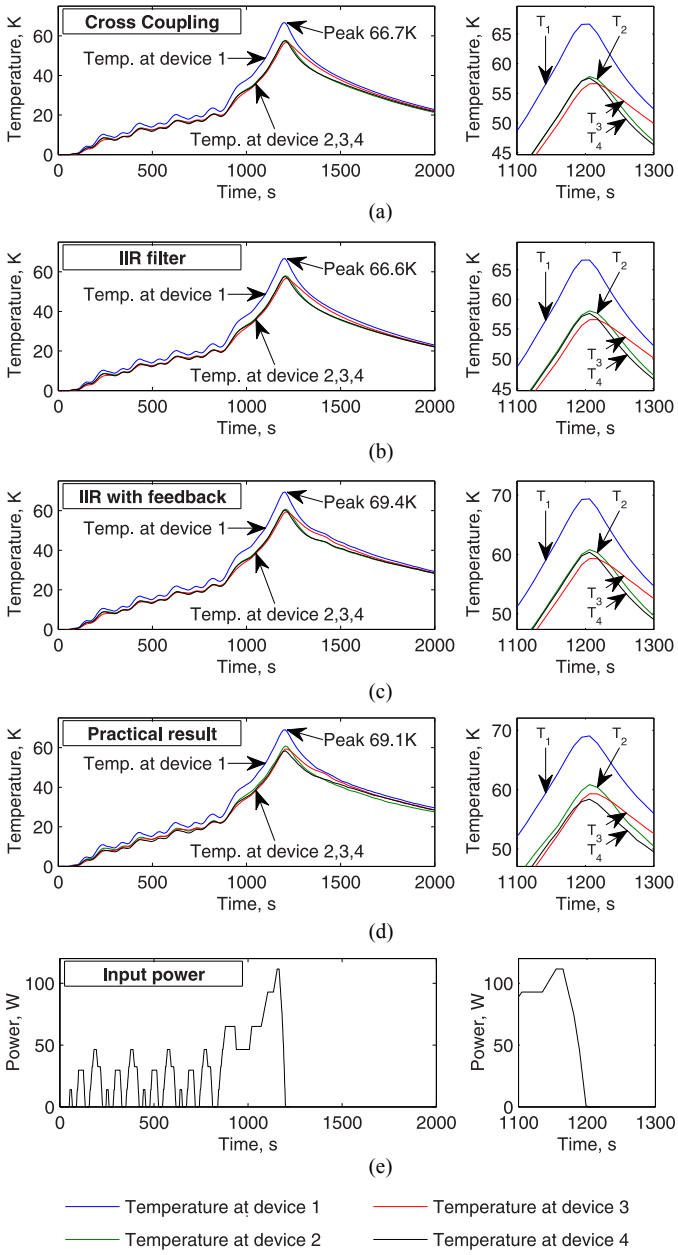

Fig. 11. Temperature responses for an arbitrary power waveform. (a) Response from frequency-domain cross coupling. (b) Response from fitted IIR filter. (c) Response from feedback-corrected IIR filter (with feedback from θ_3). (d) Practical result. (e) Input power.

temperature response is shown in Fig. 11(d). In each case, the same power was applied to each device. The left-hand side of each figure shows the response over an extended period, while the right-hand side shows detail around the peak temperature point.

There is good correlation between all predicted responses and the practical response. The shapes of the curves show excellent agreement with the practical result. This is most evident around the temperature peak, where only a minor difference in the relative positions of T_2 and T_4 can be seen. This error is likely to relate to a minor change in the ambient conditions between the

TABLE I
ACCURACY OF PREDICTIONS USING DIFFERENT METHODS COMPARED TO PRACTICAL RESULT

	Root-mean-square error from practical result (K)			
	At T_1	At T_2	At T_3	At T_4
Cross coupling	4.0	3.7	3.7	3.8
Fitted IIR filter	3.8	3.4	3.7	3.7
Feedback-corrected IIR	0.47	0.54	0[a]	0.51

[a] by definition

characterization of the system and the practical result measurement. The error is apparent in all three predictions because each result is derived from the same cross coupling characteristics and input-power waveforms. There is little difference in waveform shape produced between the three prediction methods, demonstrating their equivalency.

The root-mean-square error between each prediction method and the practical result is given in Table I. Cross coupling and fitted IIR filter results both show around a 4 K error in each temperature reading, which corresponds to 6% of the peak temperature. This error is significantly reduced by feedback from the temperature of device 3 to around 0.5 K, which corresponds to 1% of the peak temperature.

The computational requirements of the prediction techniques are compared in Table II. These figures are for a sequence of 174 time steps, where a further 334 are required for settling time padding in the direct cross coupling calculation, making the sequence length 512 for efficient Fourier transform calculation. The direct cross coupling procedure is significantly more complex than using a fitted IIR filter since the required number of multiplication–additions to calculate the entire temperature response is an order of magnitude higher. In addition complex number arithmetic is required since most of these operations are part of a DFT, further increasing computational complexity.

The difference is more significant if only a single time step is to be calculated. In this case, the direct cross coupling procedure still requires that the whole sequence is processed, which means there is no reduction in required resources. However, for the IIR filter, only a single iteration is required. The result is three orders of magnitude difference in calculation complexity.

The difference in required storage also demonstrates an advantage of the IIR filter, which requires only the seven element filter state vector to be stored per cross coupling characteristic for the direct form II implementation [18], whereas the cross coupling requires the length of both the padded sequence and its DFT to be stored simultaneously during the DFT. These figures neglect the need to store the cross coupling characteristics, which are also smaller in the case of the IIR filter, in that case consisting only of ten variables in vectors $\boldsymbol{a}$ and $\boldsymbol{b}$ combined.

To relate these resource requirements to a practical situation, the timing requirements for a standard microcontroller were calculated. For the direct cross coupling calculation, processor time is dominated by the calculation of the DFTs, which requires 178 ms for a forward transform and 196 ms for an inverse transform when implemented using fixed-point arithmetic on an

TABLE II
MICROPROCESSOR RESOURCES REQUIRED PER CROSS COUPLING CHARACTERISTIC CALCULATED

	To calculate one time step		To calculate entire sequence	
	Multiplication-additions	Variables stored	Multiplication-additions	Variables stored
cross coupling	10 750[b]	1024	10 750[b]	1024
Fitted IIR filter[c]	11	7	1914	7

[b] Assuming a DFT requires $n_s \log_2 n_s$ multiplication–additions for an n_s-length sequence.
[c] With or without feedback correction.

ATmega1284P clocked at 10 MHz. Each calculation, therefore, takes 374 ms. By comparison, 174 iterations of the IIR filter requires 416 μs with or without feedback. These figures relate to calculating the response per cross coupling characteristic. For the arrangement in this paper, four temperatures are calculated from four power inputs, meaning that more than four times these resources are required.

From this data, it is clear that the fitted IIR filter is significantly more computationally efficient than using the direct cross coupling procedure. If the direct cross coupling procedure is used, at least half of processor time is required for temperature prediction. Using the proposed filter technique releases this processor time for other tasks, such as temperature prediction under several possible future loads or electrical management of the system. With the addition of feedback temperature correction, a very close prediction of the temperature response can be made.

VII. CONCLUSION

A technique to predict the temperature response of a multielement thermal system has been presented. Initially, a characterization was performed using a PRBS technique, calculating the complex frequency-domain cross coupling. Subsequently, the characteristics can be used to predict the device temperature responses for a known input-power waveform. The resulting prediction generated by the presented method shows good agreement with the practical system used for evaluation. To reduce the computational complexity of the initial method, a digital IIR filter is fitted to each cross coupling characteristic. An excellent correlation is demonstrated that produces a near-identical temperature response compared to the direct cross coupling procedure. Further temperature responses can be extrapolated by inputting expected future values to the filter. Experimental validation on the practical system shows good agreement between IIR filter predictions and practical results. This agreement can be substantially improved by taking feedback from a reference temperature.

REFERENCES

[1] M. Yilmaz and P. Krein, "Review of integrated charging methods for plug-in electric and hybrid vehicles," in *Proc. IEEE Int. Conf. Veh. Electron. Safety*, Istanbul, Turkey, 2012, pp. 346–351.

[2] T. Brückner and S. Bernet, "Estimation and measurement of junction temperatures in a three-level voltage source converter," *IEEE Trans. Power Electron.*, vol. 22, no. 1, pp. 3–12, Jan. 2007.

[3] G. C. James, V. Pickert, and M. Cade, "A thermal model for a multichip device with changing cooling conditions," in *Proc. 4th IET Conf. Power Electron., Mach. Drives*, Apr. 2008, pp. 310–314.

[4] H. Wang, S. X.-D. Tan, G. Liao, R. Quintanilla, and A. Gupta, "Full-chip runtime error-tolerant thermal estimation and prediction for practical thermal management," in *Proc. IEEE/ACM Int. Conf. Comput.-Aided Des.*, Nov. 2011, pp. 716–723.

[5] P. L. Evans, A. Castellazzi, and C. M. Johnson, "Automated fast extraction of compact thermal models for power electronic modules," *IEEE Trans. Power Electron.*, vol. 28, no. 10, pp. 4791–4802, Oct. 2013.

[6] X. Wang, K. Ma, and Y. Wang, "Adaptive power control with online model estimation for chip multiprocessors," *IEEE Trans. Parallel Distrib. Syst.*, vol. 22, no. 10, pp. 1681–1696, Oct. 2011.

[7] M. Musallam and C. M. Johnson, "Real-time thermal models for health management of power electronics," *IEEE Trans. Power Electron.*, vol. 25, no. 6, pp. 1416–1425, Jun. 2010.

[8] J. W. Kolar, U. Drofenik, J. Biela, M. L. Heldwein, H. Ertl, T. Friedli, and S. D. Round, "PWM converter power density barriers," in *Proc. Power Convers. Conf. - Nagoya*, Apr. 2007, pp. 9–29.

[9] J. N. Davidson, D. A. Stone, M. P. Foster, and C. R. Gould, "Prediction of device temperatures in an electric vehicle battery charger system by analysis of device thermal cross coupling," in *Proc. 15th Eur. Conf. Power Electron. Appl.*, Lille, France, Sep. 2013, pp. 1–9.

[10] W. D. T. Davies, *System Identification for Self-Adaptive Control*. London, U.K.: Wiley, 1970, pp. 44–88.

[11] J. N. Davidson, D. A. Stone, and M. P. Foster, "Required Cauer network order for modelling of thermal transfer impedance," *Electron. Lett.*, vol. 50, no. 4, pp. 260–262, Feb. 2014.

[12] M. Salleras, M. Carmona, and S. Marco, "Issues in the use of thermal transients to achieve accurate time-constant spectrums and differential structure functions," *IEEE Trans. Adv. Packag.*, vol. 33, no. 4, pp. 918–923, Nov. 2010.

[13] A. J. Fairweather, M. P. Foster, and D. A. Stone, "Battery parameter identification with Pseudo random binary sequence excitation (PRBS)," *J. Power Sources*, vol. 196, pp. 9398–9406, 2011.

[14] A. J. Saavedra-Montes, J. M. Ramirez-Scarpetta, O. P. Ramos-Paja, and C. A. Malik, "Identification of excitation systems with the generator online," *Electric Power Syst. Res.*, vol. 87, pp. 1–9, Jun. 2012.

[15] J.-D. Gabano and T. Poinot, "Fractional modelling and identification of thermal systems," *Signal Process.*, vol. 91, no. 3, pp. 531–541, Mar. 2011.

[16] J. N. Davidson, D. A. Stone, M. P. Foster, and D. T. Gladwin, "Improved bandwidth and noise resilience in thermal impedance spectroscopy by mixing PRBS signals," *IEEE Trans. Power Electron.*, vol. 29, no. 9, pp. 4817–4828, Sep. 2014.

[17] N. V. Queipo, J. A. C., Humphrey, and A. Ortega, "Multiobjective optimal placement of convectively cooled electronic components on printed wiring boards," *IEEE Trans. Compon., Packag. Manuf. Technol.*, vol. 21, no. 1, pp. 142–153, Mar. 1998.

[18] A. V. Oppenheim and R. W. Schafer, *Discrete-Time Signal Processing*. Englewood Cliffs, NJ, USA: Prentice-Hall, 1999, pp. 345–418, 510–511, 559–561, 576.

[19] S. Sirisukprasert, L. Jih-Sheng, and L. Tian-Hua, "Optimum harmonic reduction with a wide range of modulation indexes for multilevel converters," *IEEE Trans. Ind. Electron.*, vol. 49, no. 4, pp. 875–881, Aug. 2002.

[20] P. R. Strickland, "The thermal equivalent circuit of a transistor," *IBM J. Res. Develop.*, vol. 3, no. 1, pp. 35–45, Jan. 1959.

[21] M. M. Gouda, S. Danaher, and C. P. Underwood, "Quasi-adaptive fuzzy heating control of solar buildings," *Building Environ.*, vol. 41, no. 12, pp. 1881–1891, Dec. 2006.

[22] A. Ridge, R. McMahon, and H.-P. Kelly, "Detailed thermal modelling of a tubular linear machine for marine renewable generation," in *Proc. IEEE Int. Conf. Ind. Technol.*, Feb. 2013, pp. 1886–1891.
[23] J. D. Holmes, M. P. Foster, and D. A. Stone, "System-wide temperature estimation for IMS based power electronics circuits," in *Proc. Power Electron. Drive Syst. Int. Conf.*, Nov. 2009, Taipei, Taiwan, pp. 615–618.
[24] R. C. Dorf Ed., *The Electrical Engineering Handbook*, 2nd Ed. Boca Raton, FL, USA: CRC Press, 1997, pp. 239–254.
[25] J. N. Davidson, D. A. Stone, and M. P. Foster, "Minimum gain identifiable when pseudorandom binary sequences are used for system identification in noisy conditions," *Electron. Lett.*, vol. 49, no. 22, pp. 1388–1389, Oct. 2013.
[26] MathWorks. (2013, Jul. 8). MATLAB 2013a documentation: invfreqz [Online]. Available: http://www.mathworks.co.uk/help/signal/ref/invfreqz.html
[27] Anon, "Directive 90/C81/01," *EEC J. Officiel No. C81*, p. 110, Mar. 30, 1990.

Jonathan N. Davidson received the M.Eng. degree in electronic engineering from the University of Sheffield, Sheffield, U.K., in 2010. Since 2010, he has been working toward the Ph.D. degree at the Department of Electronic and Electrical Engineering, University of Sheffield.

His current research interests include thermal modeling and management of power electronics.

Mr. Davidson is a Member of the Institution of Engineering and Technology.

David A. Stone received the B.Eng. degree in electronic engineering from the University of Sheffield, Sheffield, U.K., in 1984, and the Ph.D. degree from Liverpool University, Liverpool, U.K., in 1989.

He returned to the University of Sheffield as a Member of academic staff specializing in power electronics and machine drive systems. His current research interests include hybrid-electric vehicles, battery management, electromagnetic compatibility, and novel lamp ballasts for low-pressure fluorescent lamps.

Martin P. Foster received the B.Eng. degree in electronic and electrical engineering, the M.Sc. degree in engineering in control systems, and the Ph.D. degree for his thesis "Analysis and Design of High-order Resonant Power Converters" from the University of Sheffield, Sheffield, U.K., in 1998, 2000, and 2003, respectively.

In 2003, he became a Member of academic staff at Sheffield specializing in power electronic systems and was made a Senior Lecturer in 2010. His current research interests include the modeling and control of switching power converters, resonant power supplies, multilevel converters, battery management, piezoelectric transformers, power electronic packaging, and autonomous aerospace vehicles.